A Simple Assembly Planner for the Insertion of Ring-shaped Deformable Objects

Ixchel G. Ramirez-Alpizar *†, Kensuke Harada† and Eiichi Yoshida††

†Department of Systems Innovation, Graduate School of Engineering Science, Osaka University, Osaka, Japan
††CNRS-AIST JRL (Joint Robotics Laboratory), UMI3218/RL, National Institute of Advanced Industrial Science and Technology (AIST), Ibaraki, Japan

November 13, 2017

Abstract

Purpose - The aim of this work is to develop a simple planner able to automatically plan the motion for a dual-arm manipulator that assembles a ring-shaped elastic object into a cylinder. Moreover, it is desirable to keep the amount of deformation as small as possible, since stretching the object can permanently change its size thus failing to perfectly fit in the cylindrical part and generating undesired gaps between the object and the cylinder.

Design/methodology/approach - The assembly task is divided in two parts: assembly task planning and assembly step planning. The first one computes key configurations of the robot's end-effectors and it is based on a simple heuristic method, while the latter computes the robot's motion between key configurations using an optimization-based planner that includes a potential-energy-based cost function for minimizing the object's deformation.

Findings - The optimization-based planner is shown to be effective for minimizing the deformation of the ring-shaped object. A simple heuristic approach is demonstrated to be valid for inserting deformable objects into a cylinder. Experimental results show that the object can be kept without deformation for the first part of the assembly task thus reducing the time it is being stretched.

Originality/value - A simple assembly planner for inserting ring-shaped deformable objects was developed and validated through several experiments. The proposed planner is able to insert ring-shaped objects

*ramirez@sys.es.osaka-u.ac.jp

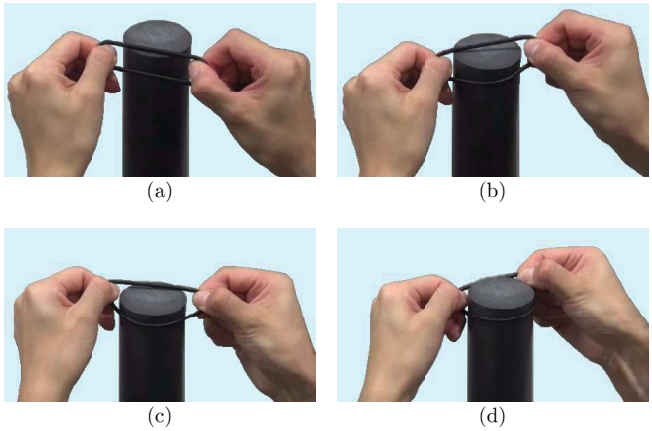

(a) (b) (c) (d)

Figure 1: Assembly process of a ring-shaped deformable object performed by a human in four steps, (a) step 1, (b) step 2, (c) step 3 and (d) step 4.

without using any sensor (visual and/or force) feedback. The only feedback used is the position of the robot's end-effectors, which is usually available for any robot.

1 Introduction

In the last decades, the development and/or improvement of all kind of sensors, vision systems, grippers, etc., has allowed robots to manipulate several types of objects, such as ropes, wires (Wakamatsu, Hirai, & Iwata 2004), food products (Friedrich et al. 1996, Sakamoto et al. 2007), etc. This has contributed to the widespread use of industrial robots at factories to automatize manufacturing processes. However, many assembly processes remain a challenging task for robots, since they require mating (fastening) two or more parts. In the particular case of assembly processes involving deformable objects, this can be attributable to the high dexterity needed to manipulate these kinds of objects. In contrast, we (humans) possess (or we are able to get through experience) the dexterity required to handle objects of several types of materials, shapes, sizes, etc., and we also have very fine tactile and vision senses to perform precision and assembly tasks.

In this work, we consider the assembly process of inserting a ring-shaped elastic object into a cylinder as a first step on the manipulation of deformable objects in assembly tasks. This type of assembly is commonly used in the manufacturing process of machines for sealing pipes against liquids or gases, to prevent any leakage. For example, ring-shaped elastic objects commonly known as "o-rings" or packing are frequently used at the automotive industry for the manufacture of engines, fuel systems, air conditioning, transmission, etc., to seal against oil, fuel, air, among others. These o-rings have smaller diameters than the pipes (cylinder) they are used in; thus, creating pressure

against the pipe and consequently leaving no gap between them and the pipe. Also, they are usually made of materials with relatively high stiffness to endure time, application temperatures and pressure. These inherent features of o-rings have two important implications in assembly tasks. First, large deformations (stress) lead to its deterioration and/or fracture, e.g. the o-ring is not able to return to its original size, thus generating undesired gaps with the pipe, leading to leakage and failures[1]. Second, a considerable amount of force is needed to generate large deformations. Consequently, it is very important to keep the object's deformation as small as possible. For this problem, this paper proposes a simple method that can easily and effectively reduce the amount of elastic deformation during the assembly process.

The goal of this work is to develop a planner able to automatically plan the motion for a dual-arm manipulator that inserts an elastic object into a cylinder. To achieve this goal, we have to solve the following two problems: first, to accomplish the assembly of a ring-shaped elastic object as shown in Fig. 1, a series of key poses for a robot has to be determined, we call this process "assembly task planning". Second, we have to plan the motion of the robot connecting each pair of key poses and we call this process "assembly step planning". For the latter problem, we considered a motion planner based on optimization techniques.

Zucker et al. (2013) proposed an algorithm called Covariant Hamiltonian Optimization and Motion Planning (CHOMP) based on the gradient descent optimization technique where the choice of the objective function and the terminal condition of the optimization process is free. Thus, it can be expected that the motion planning for manipulating elastic objects with complex deformations could be easily achieved by adding an elastic energy related term to the objective function of CHOMP. Like this, it would be relatively simple to obtain an optimized path over different cost functions (collision, smoothness, elastic energy of the object, etc.) rather than using sampling-based path planning methods where the path obtained is asymptotically optimal (Karaman & Frazzoli 2011). Taking into account computational costs, the CHOMP algorithm is more efficient in the time spent per iteration than stochastic optimization planners such as STOMP (Kalakrishnan et al. 2011), which is convenient if the optimization function is non-differentiable or non-smooth.

In our previous work, we proposed an object's elastic energy related term (included into the optimization problem of CHOMP) for the motion planning of a two-arm robot towards the insertion of an elastic ring-shaped object into a cylinder (Ramirez-Alpizar et al. 2014). We also introduced a less strict collision cost function than the originally proposed by Zucker et al. (2013), which is necessary to allow the manipulator to be as near as possible to the cylinder without colliding with it, and presented a simulation analysis of the objective functional weights. Extending our previous work, in this paper we first introduce an assembly task planning algorithm that focuses on how to successfully

[1]NASA's space shuttle *Challenger* explosion in 1986 was determined to be due to an o-ring failure (Atkinson 2012)

assemble a ring-shaped object to a cylinder without using visual feedback, reducing the computational cost of our assembly planner. This simple search algorithm computes the next feasible key pose (partial goal configuration) of the manipulator's gripper, taking into consideration the object's deformation and the position/orientation of the robot's end effector at each assembly step, avoiding the accumulation of possible positioning errors. In addition to the simulation analysis showing the influence of the optimization weights, we show the experimental results carried out on a Baxter Research Robot[2] using a common rubber band, a silicon-made o-ring, and a nitrile-made o-ring to demonstrate the validity of the proposed assembly planner.

This paper is organized as follows: in section 2, we briefly review related work. In section 3, we give the outline of the assembly problem discussed in this work. In section 4, we introduce the planning algorithm for the assembly task of a ring-shaped object into a cylinder. In section 5, we give a brief introduction to the CHOMP algorithm and introduce an energy-based objective functional to minimize the deformation of the object. In section 6, we show the simulation results of the proposed assembly planner. In section 7, we show the experimental results of assembling three different ring-shaped objects using the Baxter robot. In section 8, we give the conclusion of this work.

2 Related Work

2.1 Motion Planning

Motion planning has been a very active research area in robotics in the past decades. Among the most popular algorithms are Probabilistic Road Maps (Karaman & Frazzoli 2011), Rapidly-exploring Random Trees or RRT (LaValle & Kuffner Jr 2001), the RRT* (Karaman & Frazzoli 2010) among others. In contrast, optimization-based planners such as CHOMP (Zucker et al. 2013) and STOMP (Kalakrishnan et al. 2011) have been developed to tackle smoothness problems when using sampling-based planners. More recently, Shoushtari et al. (2016) proposed a motion planner using a bio-mimetic approach, where human arm movements are taken into account to generate the motion control of a redundant manipulator. For an extensive review on robot motion planning approaches the reader is refer to Masehian & Sedighizadeh (2007) review.

2.2 Manipulation of Deformable Objects

Towards the challenging topic of manipulating deformable objects, different work has been done, particularly for flexible linear objects, such as ropes, cables, etc. Yamakawa et al. (2010) have discussed the motion planning for knotting linear flexible objects, where a model for the linear object is derived and used for the motion planning of the robot to dynamically knot the object, and for the deformation control of a flexible rope (Yamakawa et al. 2012). Wakamatsu et al.

[2] http://www.rethinkrobotics.com/baxter/

have discussed manipulation plans for knotting and unraveling linear objects by representing the object as a series of crossing states, and based on these states the manipulation plan is determined (Wakamatsu, Tsumaya, Arai & Hirai 2004, Wakamatsu et al. 2006). Vinh et al. (2012) have shown a strategy for knotting a deformable rope using a Wii controller as teaching pennant. Wang et al. (2015) have shown a process to design fixtures to arrange and tighten two types of knots and unknots by three different methods. Saha & Isto (2007) have discussed the motion planning for knotting linear deformable objects around static objects using what they called "topologically biased" probabilistic roadmap in the configuration space of the linear deformable object. Rambow et al. (2012) have discussed the task of changing the starting configuration of a deformable tube to a given goal configuration. This is achieved by analyzing a human demonstration of the same task and then transferring it to the robot. Lamiraux & Kavraki (2001) proposed a motion planner based on a probabilistic roadmap (Kavraki et al. 1996) that is able to change the initial configuration of an elastic object into a desired goal configuration under manipulation constraints. Moll & Kavraki (2006) proposed a path planner that computes a stable configuration of deformable linear objects based on a sampling-search method. Bretl & McCarthy (2014) have discussed the quasi-static manipulation of planar elastic rods using a sampling-based planning algorithm similar to the one proposed by Moll & Kavraki (2006) where the planar elastic rod is held by a robotic gripper and the sampling space is defined as the set of equilibrium configurations of the elastic rod. Most of the work involving deformable objects have only discussed linear deformable objects (LDO), i.e. ropes, cables, tubes, etc., however few work have been done on the manipulation planning for ring-shaped deformable objects (Yoshida et al. 2015). While the configuration of LDO objects can be estimated by the position of its ends (two points), the configuration of ring-shaped deformable objects cannot be estimated with the same ease (need more than two points) and it requires more complex methods, such as Finite Element Methods.

2.3 Assembly of Deformable Objects

There has been work specifically discussing assembly tasks for flexible parts, which has mainly focused on the insertion of a flexible beam (Zheng et al. 1991) and a flexible wire (Nakagaki et al. 1997) on a rigid hole. Yue & Henrich (2002) have studied the insertion of a vibrating linear deformable object into a hole by using a force/torque sensor mounted on the robot's wrist. Wolter & Kroll (1996) have discussed a general assembly task of a toy called "launcher" and focused on the push, pull and knot (form into a loop) of strings. Besides the manipulation of LDOs, Villareal & Asada (1991) have presented a methodology for planning assembly tasks involving compliant parts with bounded geometric uncertainties. Miura & Ikeuchi (1995, 1998) have discussed the assembly of a rubber belt and fixed pulleys, where a rubber belt is inserted into a small pulley, and then the belt is stretch so as to be inserted into a bigger pulley. However, as far as we know, there has been no work discussing the assembly planning for

the insertion of ring-shaped elastic objects, a task that is done by humans and is frequently used by the manufacturing industry, as explained in section 1.

3 Problem Formulation

Consider the assembly motion planning of a ring-shaped elastic object into a cylinder, as shown in Fig. 1. A cylinder is fixed at the center between both arms of a robot and the assembly task starts with the robot holding the object with both grippers. The undeformed diameter of the ring-shaped object is smaller than that of the cylinder, implying that the object must be stretched in order to be inserted into the cylinder, so as to perfectly fit in the cylinder to avoid any gap (as explained in section 1). Furthermore, we make the following assumptions:

1) The manipulator grasps firmly the elastic object.
2) The grasping point of the elastic object with respect to the manipulator's wrist coordinate system is known and constant.
3) The size, shape and Young's Modulus of the object are known.
4) The cylinder used for the assembly task is static, rigid and its position and dimensions are known.

The ring-shaped object is considered as two springs s_{in} and s_{out} connected in series (closing the loop), as shown in Fig. 2. The connection points are assumed to be at the grasping points by the robot's grippers such that the undeformed lengths $l_{0\text{in}}$ and $l_{0\text{out}}$ of each of the springs are:

$$l_{0\text{in}} = l_{0\text{out}} = \frac{1}{2} L_0 \ , \tag{1}$$

where $L_0 = \pi d_{\text{ring}}$, and d_{ring} is the undeformed diameter of the ring-shaped object. The shape of the object can be approximated based on an estimation of whether the object has made contact with the cylinder or not. Contact is estimated based on the geometric relationship between the position of the robot's grippers (grasping points) and the cylinder (a detailed explanation is given in section 5.2). Once the object's shape has been approximated, the deformation of each of the springs can be computed and it can also be evaluated whether the object has been inserted or not into the cylinder.

We divide the assembly motion planning in two procedures: the first one will compute a robot's key pose based on the robot's grippers position and the object's deformation, we call this procedure "assembly task planning" (detailed in section 4). The second procedure will plan the motion of the robot between its current position and the next key pose computed in the first procedure and we call it "assembly step planning" (detailed in section 5). As will be explained in the following section, the assembly task planning procedure is in charge of evaluating and deciding if the assembly process has successfully finished.

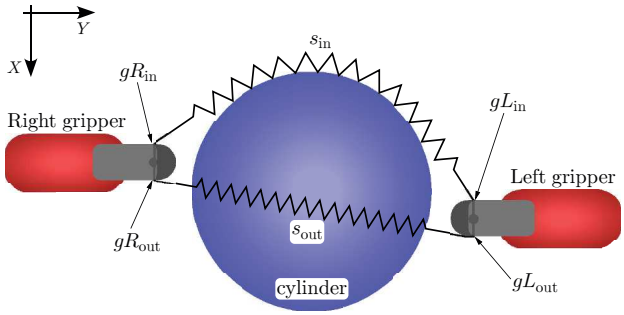

Figure 2: Top view of the modeled ring-shaped object hold by the robot's grippers.

4 Assembly Task Planning

In this section we explain the assembly method proposed for inserting a ring-shaped elastic object into a cylinder. Similarly to the assembly motion done by a human (Fig. 1), the robot first approaches a part of the ring-shaped object at one side of the cylinder, then the robot pulls the object and inserts the rest of the object by moving the hands towards the opposite side of the starting position.

We divide the assembly process in several steps where only one of the arms moves at each step, alternating between left and right arms. The assembly task planner will begin a new step by first computing the next key pose for the robot's gripper (beginning with the left arm at step 1). Then, it will send this key pose to the motion planner (section 5) which will search for an inverse kinematics solution using the Kinematics and Dynamics Library (KDL), then it will compute the path to be executed by the robot and will send back to the assembly task planner the current position of the robot (after executing the given path). Based on the information received, the assembly task planner will evaluate and decide if the ring-shaped object has been inserted.

4.1 Key Pose

To determine the next key pose (grasping point $P_{i+1} \in \mathbb{R}^3$) of the gripper at each step, we implemented the procedure described in Algorithm 1 (i-th step). This procedure is based on the grippers' current positions and the cylinder information which gives robustness to our planner in the sense that even if the gripper does not move to the exact desired position, in the next step the planner will start from the current position and will not accumulate positioning errors. Algorithm 1 is basically searching for the closest point to move the robot's grippers a given minimum distance. The grasping point of the object by the grippers at the end of step i is represented by P_i, $z_{\min}$ is the minimal height to ensure the assembly of the object and $\text{sgn}(n)$ denotes the sign function of n. The angle α is the angle in the $X-Y$ plane between the Y axis and the line

Algorithm 1 Calculate next key pose $P_{i+1}(x_{i+1}, y_{i+1}, z_{i+1})$

1: $\alpha \leftarrow 0$
2: $D \leftarrow 0.2\, d_{\text{ring}}$
3: **if** $z_i > z_{\min}$ **then**
4: $\quad z_{i+1} \leftarrow z_i - dz$
5: **else**
6: $\quad z_{i+1} \leftarrow z_i$
7: **end if**
8: keep $\leftarrow$ **true**
9: **while** keep **do**
10: $\quad y_{i+1} \leftarrow y_i - (D\cos(\alpha))\ \text{sgn}(y_i)$
11: $\quad x_{i+1} \leftarrow x_{i+1} \mid D = \|P_{i+1} - P_i\|$
12: $\quad$ **if** $x_{i+1} - x_{i-1} < \Delta X$ **or** collision detected **or**
13: $\quad\quad$ position is unreachable **then**
14: $\quad\quad$ **if** $\alpha < \pi/2$ **then**
15: $\quad\quad\quad \alpha \leftarrow \alpha + \Delta\alpha$
16: $\quad\quad$ **else if** $D < D_{\max}$ **then**
17: $\quad\quad\quad D \leftarrow D + \Delta D$
18: $\quad\quad\quad \alpha \leftarrow 0$
19: $\quad\quad$ **else**
20: $\quad\quad\quad y_{i+1} \leftarrow y_{i-1} + \text{sgn}(y_{i-1}) * dy$
21: $\quad\quad\quad x_{i+1} \leftarrow x_{i-1} + dx$
22: $\quad\quad\quad$ keep = **false**
23: $\quad\quad$ **end if**
24: $\quad$ **else**
25: $\quad\quad$ keep = **false**
26: $\quad$ **end if**
27: **end while**
28: **return** P_{i+1}

connecting the grasping points of the object by both grippers $D = \|P_{i+1} - P_i\|$, as illustrated in Fig. 3.

The algorithm starts searching for a key pose (P_{i+1}) near to the current position of the opposite gripper (P_i). At first, a constant change in the z coordinate is given (dz) to determine z_{i+1}. Then, as a first try, the value of y_{i+1} is set such that the line connecting both grippers is parallel to the Y axis ($\alpha = 0$ in Fig. 3). The initial value of D is set smaller than the object's undeformed diameter (d_{ring}), and then x_{i+1} is computed such that $D = \|P_{i+1} - P_i\|$ is satisfied (Algorithm 1: line 11). The initial value of D at each step is set depending on the position of the grippers, i.e. at the beginning of the assembly is small and as the assembly progresses (the object begins to get deformed) its initial value is changed to d_{ring} and finally when it approaches the end of the assembly, its initial value is set again small. Furthermore, the choice of calculating first y_{i+1} based on α (in the $X - Y$ plane) and then x_{i+1} based on

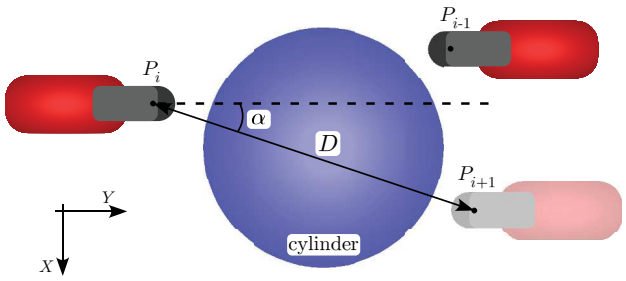

Figure 3: Top view of the cylinder and the robot's grippers at step i.

D is to ensure that the search begins with a valid y_{i+1} (not in collision with the cylinder) and with the smallest possible value for D (i.e., smallest deformation of the ring-shaped object).

Next, the algorithm checks three important conditions: 1) P_{i+1} is not in collision with the cylinder, 2) the robot can reach the position and 3) P_{i+1} is at least at a distance ΔX from the previous key pose (Algorithm 1: line 12). If any of these three conditions are not satisfied, the algorithm will increment α, recompute y_{i+1} and x_{i+1}, and check again. It will iterate until it finds a point P_{i+1} satisfying all three conditions. If α reaches its maximal value $\pi/2$, then it will increment D and reset α to zero and begin to iterate again. In the extraordinary case that D also reaches its maximal allowed value $D_{\max} = 1.2\ d_{\text{ring}}$, the algorithm will stop and will set the next key pose to a close by point in X positive direction by dx and in the outward direction from the cylinder by dy (Y axis) which should not be in collision with the cylinder (Algorithm 1: lines 20 and 21). The values of dx and dy are determined based on the tolerance error of the robot's position controller, otherwise if we choose smaller values than the tolerance error the robot will not move. ΔX plays a key role in the number of steps needed to finish the assembly task, while the limits on α and D will ensure that the object's deformation does not go beyond $1.2\ d_{\text{ring}}$ and that the assembly task is achieved successfully.

4.2 Assembly Ending Condition

At the end of each executed step, the assembly task planner will check if the ring-shaped object has been inserted. Based on the position of both grippers and under assumption 1 of section 3, it is possible to assess (with a certain degree of confidence) if the ring has been inserted by checking if there are intersecting points between the line connecting the outside grasping points gR_{out}, gL_{out} (Fig. 2) and the cylinder. If an intersecting point exists, it is determined that the object has not been inserted and the task planner proceeds to compute a new key pose. Otherwise, it will check the x and z components of gR_{out}, gL_{out} to determine if the assembly is starting or is ending. This method is valid since we do not move both arms at the same time. By moving one arm at a time it is possible to assume that the robot will follow certain trajectory (given the

"naive" initialization of the CHOMP algorithm). Therefore, given the trajectory in z direction of the grasping points, it is possible to make an educated guess that the object has been "caught" in the cylinder when the grasping points are below the cylinder's surface and ahead (in x) of its center.

5 Assembly Step Planning

In this section we describe the motion planner used to obtain the trajectory between the key poses computed by the assembly task planner explained in section 4.

5.1 CHOMP Algorithm

In this section we propose a motion planning algorithm for manipulating elastic objects, based on the algorithm developed by Zucker et al. (2013), called Covariant Hamiltonian and Motion Planning (CHOMP). This algorithm is capable of finding a smooth and collision-free trajectory ξ between two specific configurations q_0 and q_{goal} of the configuration space $\mathbb{R}^m$. The trajectory ξ is expressed as a function mapping time to robot configurations $q \in \mathbb{R}^m$. Using a uniform discretization of n time steps of length Δt, the trajectory is represented as $\xi \approx ({q_1}^T, {q_2}^T, \ldots, {q_n}^T)^T \in \mathbb{R}^{n \times m}$. The CHOMP algorithm typically starts with a simple straight line between the given configurations (even if it is not collision-free), as the initial trajectory ξ_0. Then, it optimizes the initial trajectory through an iterative update rule (Zucker et al. 2013) given by:

$$\xi_{i+1} = \xi_i - \frac{1}{\eta}(K^T K)^{-1} \bar{\nabla} \mathcal{U}(\xi_i) \tag{2}$$

where ξ_i is the refined trajectory at iteration i, K is a finite differencing matrix, η is the regularization coefficient that determines the trade-off between minimizing the objective functional $\mathcal{U}$ and the step size, and $\bar{\nabla}$ is the functional gradient operator. The objective functional $\mathcal{U}(\xi_i)$ is given by:

$$\mathcal{U}(\xi) = \mathcal{F}_{\text{obs}}(\xi) + \lambda \mathcal{F}_{\text{smooth}}(\xi) \tag{3}$$

where $\mathcal{F}_{\text{smooth}}$ is the smoothness objective that penalizes the trajectory ξ_i based on dynamical parameters such as the squared velocity norms over the trajectory, and $\mathcal{F}_{\text{obs}}$ is the obstacle objective which penalizes the robot for being near and/or in contact with the environment and/or itself.

5.2 Energy Objective Functional

In this work we employ CHOMP for the assembly manipulation of a ring-shaped elastic object. We suppose the assembly task shown in Fig. 1. The objects used in this kind of assembly process, usually have a relatively high stiffness[3]; which

[3]We refer to stiffness as the state of being difficult to bend or stretch.

as explained in section 1, have two important implications when assembling them. First, large deformations lead to its deterioration and/or fracture, e.g. the o-ring is not able to return to its original size, thus generating undesired gaps with the cylinder. Second, a considerable amount of force is needed to generate large deformations. Thus, it is very important to keep the object's deformation as small as possible. To minimize the object's deformation, we introduce an energy objective functional that penalizes the trajectory ξ_i for stretching the object. Therefore, we rewrite the objective functional of (3) as

$$\mathcal{U}(\xi) = w_{\mathrm{c}}\mathcal{F}_{\mathrm{obs}}(\xi) + w_{\mathrm{s}}\mathcal{F}_{\mathrm{smooth}}(\xi) + w_{\mathrm{e}}\mathcal{F}_{\mathrm{energy}}(\xi) \tag{4}$$

where w_{c}, w_{s}, w_{e}, are the weights of the obstacle objective, the smoothness objective and the energy objective, respectively. We employ the smoothness objective as define by Zucker et al. (2013), and the obstacle objective as described in section 5.3. We define the energy objective functional $\mathcal{F}_{\mathrm{energy}}$ as

$$\mathcal{F}_{\mathrm{energy}}(\xi) = \int_0^1 U\big(\xi(t)\big)\left\|\frac{\mathrm{d}}{\mathrm{d}t}\xi(t)\right\|\mathrm{d}t \tag{5}$$

where $U(\xi)$ is the energy cost function in the configuration space.

The functional gradient (Quinlan 1994) of the energy objective is obtained as

$$\bar{\nabla}\mathcal{F}_{\mathrm{energy}}(\xi) = \|\xi'\|\Big(\big(I - \hat{\xi}'\hat{\xi}'^{T}\big)\nabla U - U\kappa\Big) \tag{6}$$

where κ is the curvature vector (Quinlan 1994) given by

$$\kappa = \frac{1}{\|\xi'\|^2}\big(I - \hat{\xi}'\hat{\xi}'^{T}\big)\xi'',$$

$\nabla U = \partial U/\partial\xi$ is the gradient of U, and ξ' and $\hat{\xi}$ denote the time derivative and the normalized vector of ξ, respectively.

As mentioned in section 1, one important advantage of using optimization methods for motion planning is the free choice of the cost function. Consequently, for the energy cost function $U(\xi)$, we use the potential energy of a spring,

$$U(\xi) = \frac{1}{2}k x_{\mathrm{d}}(\xi)^2 \tag{7}$$

where k is the ideal stiffness of the spring, and $x_{\mathrm{d}}(\xi)$ is the deformation of the spring. In this case, we approximate the stiffness of the ring-shaped object through its Young's modulus (tensile stress by tensile strain) E as

$$k = \frac{EA_0}{L_0} \tag{8}$$

where A_0 and L_0 are the cross-sectional area and the length of the undeformed object, respectively.

Object's deformation

The deformation of the object x_{d} is approximated as:

$$x_{\mathrm{d}} = l_{\mathrm{in}} + l_{\mathrm{out}} - L_0, \tag{9}$$

where l_{in} and l_{out} are the length of the springs s_{in} and s_{out} (Fig. 2), respectively.

As discussed in section 4.2, the deformation of the object is computed under the assumption that the object gets "caught" in the cylinder when the grasping points are below the cylinder's surface and ahead (in x) of its center. First it is checked if the object has been stretched by verifying if:

$$2\big(\|P_{i+1} - P_i\| + g_{\mathrm{w}}\big) > L_0, \tag{10}$$

where g_{w} is the width of the gripper at the grasping point. If the object is being stretched, then it is determined if s_{in} has made contact with the cylinder by checking if there are intersecting points between the line connecting the inside grasping points gL_{in}, gR_{in} (Fig. 2) and the cylinder. If there are no intersecting points, it is considered that there is no contact between s_{in} and the cylinder, thus

$$l_{\mathrm{in}} = \|gR_{\mathrm{in}} - gL_{\mathrm{in}}\| + g_{\mathrm{w}}. \tag{11}$$

In the case where there are intersecting points, it is determined that s_{in} has made contact with the cylinder and the corresponding contact points (pc_1, $pc_2 \in \mathbb{R}^3$) are computed. Since it is already known that the object has been stretched, we know that the lines between the inside grasping points and the contact points are tangent lines to the cylinder (at pc_1, pc_2). Thus, we can approximate the length of s_{in} as

$$l_{\mathrm{in}} = \|gR_{\mathrm{in}} - pc_2\| + \|gL_{\mathrm{in}} - pc_1\| + l_{\mathrm{arc}} + g_{\mathrm{w}}, \tag{12}$$

where l_{arc} is the arc length between the contact points pc_1 and pc_2.

Similarly to s_{in}, it is determined if s_{out} is in contact with the cylinder. If there are no intersecting points between the cylinder and the line connecting the outside grasping points gL_{out}, gR_{out}, or if these are above the surface of the cylinder, it is considered that there is no contact between s_{out} and the cylinder, and thus

$$l_{\mathrm{out}} = \|gR_{\mathrm{out}} - gL_{\mathrm{out}}\| + g_{\mathrm{w}}. \tag{13}$$

Otherwise, the intersecting points (pc_3, $pc_4 \in \mathbb{R}^3$) are computed. Depending on the height z of gR_{out} and gL_{out} it is determined if s_{out} has made contact with the cylinder and in how many points (n). Finally, s_{out} is segmented in $n+1$ lines and we can approximate the length of s_{out} as

$$l_{\mathrm{out}} = g_{\mathrm{w}} + \sum_{j=1}^{n+1} ls_j, \tag{14}$$

where ls_j is the length of the j-th segment of s_{out}. Like this, the deformation of the ring-shaped object is approximated by computing the deformations of springs s_{in} and s_{out} based only in the position of the grasping points and the cylinder.

5.3 Collision Cost Function

Next, we consider modifying the collision cost function such that the CHOMP algorithm can be used for the assembly motion planning of elastic parts. The obstacle objective in (4) is given by (Zucker et al. 2013)

$$\mathcal{F}_{\text{obs}}(\xi) = \int_0^1 \int_{\mathcal{B}} c\Big(x\big(\xi(t),u\big)\Big) \left\| \frac{\mathrm{d}}{\mathrm{d}t} x\big(\xi(t),u\big)\right\| \mathrm{d}u\,\mathrm{d}t, \tag{15}$$

where $\mathcal{B} \subset \mathbb{R}^3$ is the set of points on the exterior body of the robot and x denotes the forward kinematics mapping a robot configuration q and a particular body point u to a point $x(q,u)$ in the workspace, and c is a workspace collision cost function that penalizes the robot for being inside or near the environment given as

$$c(x) = \begin{cases} -d(x) + \frac{1}{2}\varepsilon, & \text{if } d(x) < 0 \\ \frac{1}{2\varepsilon}\big(d(x)-\varepsilon\big)^2, & \text{if } 0 \le d(x) \le \varepsilon \\ 0, & \text{otherwise} \end{cases} \tag{16}$$

where $d(x)$ is the distance from a point x to the boundary of the nearest obstacle and ε is the collision threshold. Here, we would like to emphasize that the collision cost function is given in the workspace, since it evaluates the distance between a robot's body part and the environment. However, in the case of the energy cost in (7), as we seek to minimize the object's deformation, we use the configuration space to directly obtain the position of both grasping points and evaluate the object's deformation.

In section 6 we will show that using the collision cost function given by (16) yields indeed a collision free trajectory. However, this collision cost pushes away the trajectory needlessly far from a possible collision with the environment (cylinder), thus stretching the ring-shaped object more than two times its original size which may result in the undesired release of the ring-shaped object and in the assembly task failure.

In our case, as we want to avoid collisions with the environment and at the same time minimize the deformation of the elastic object, we need to have a balance between the collision cost function and the energy cost function (section 5.2). For this reason, we define the collision cost function as follows,

$$c(x) = \begin{cases} \frac{1}{2}\varepsilon\big(d(x)-\varepsilon\big)^2, & \text{if } d(x) < d_{\text{clear}} \\ 0, & \text{otherwise} \end{cases} \tag{17}$$

where we define d_{clear} as the minimum distance between the boundary of a body point and the boundary of the nearest obstacle, before being in collision. With

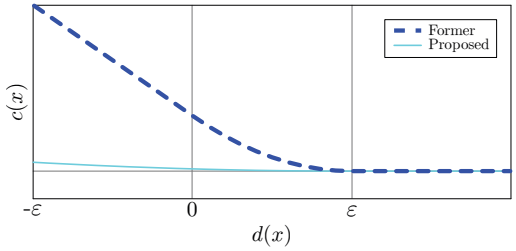

Figure 4: Comparison between collision cost functions $c(x)$, when $d_{\text{clear}} = \varepsilon$.

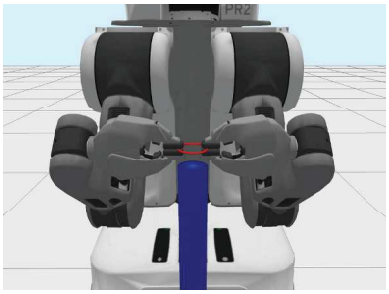

Figure 5: Initial state of the PR2 robot in simulation.

this collision cost function, the robot is able to move as near as allowed by d_{clear} to the environment.

Fig. 4 shows the plot of the original collision cost function given by (16) and the plot of the proposed collision cost function given by (17), for a fair comparison we let $d_{\text{clear}} = \varepsilon$. Note that if $d_{\text{clear}} < \varepsilon$, $c(x)$ will become zero faster, but the rest of the function is the same as the one depicted in Fig. 4. It can be seen that the original cost function rapidly increases as the distance to the obstacle gets smaller, while the proposed cost function increases with a difference of $1/\varepsilon^2$ times the original one (when $d(x) < 0$ and $\varepsilon < 1$). Therefore, even for very small values of ε (e.g. 1×10^{-6}) the value of $c(x)$ when $d(x) > 0$, will not change significantly. Only when the robot is not in collision ($d(x) > 0$) we could get similar values of $c(x)$ for the original cost function using small values of ε and the proposed one.

6 Simulation Analysis

In this section we present the simulation analysis conducted to demonstrate the validity of our assembly planner. First, we make a brief description of the simulation environment used and then we discuss the influence of the objective functionals' weights in (4).

6.1 Simulation setting

The Robot Operating System (ROS) platform and the Gazebo simulator are used to carry out the simulation of the PR2 robot handling an elastic object (approximated by rigid cylindrical links connected by rotational and translational joints). We consider the assembly of a ring-shaped object into a cylinder located at the center between the arms of the robot. Fig. 5 shows the initial state from which the assembly process starts. The ring-shaped elastic object has an inner radius of 49.9 mm, a thickness of 3 mm and a Young's modulus of $E = 4.125$ MPa. The cylinder has a radius of 50 mm.[4] Also, we added a condition to the step planner (CHOMP algorithm) to be able to "always" obtain a collision-free trajectory. Therefore now, the step planner will discard those trajectories with smaller costs that are in collision and will only consider collision-free trajectories.

Fig. 6 shows the simulation results of the assembly process carried out using the proposed assembly planner, where each snapshot shows the achieved position at each assembly step by the PR2 robot. The assembly process is accomplished in 6 steps for $\Delta X = 0.02$ and $dz = 0.007$ in the assembly task planner, and it begins by moving the left arm at step 1 (Fig. 6(a)), and finishes with the right arm at step 6 (Fig. 6(f)).

To discuss the importance of the collision cost function, we set $w_{\mathrm{e}} = 0$ in (4) (no consideration of the object's deformation). Fig. 7 shows the top view (X-Y plane) in (a) and the front view (Y-Z plane) in (b), of the trajectory described by the grasping position of the left gripper during step 3 of the assembly process, where the shaded area represents the cylinder. In Fig. 7, we compare the trajectory obtained using the original CHOMP's collision cost in (16) which we call "former" (dashed line), and the trajectory obtained using (17) which we call "proposed" (continuous line). As a first attempt we choose a collision weight of $w_{\mathrm{c}} = 10.0$ which yields a collision cost smaller than the original one. It can be seen that the grasping position trajectory obtained from the original CHOMP makes a big turn around the cylinder, while the trajectory obtained through the proposed collision cost function considerably shortens the turn around the cylinder. We must point out that for some of the assembly steps, when the given goal position for the gripper is very close to the cylinder, the original CHOMP was not able to yield a collision-free trajectory (using the same collision threshold ε and the same number of allowed iterations), since pulling the trajectory far from the object implies a considerable increase in the length of the trajectory therefore increasing its cost. In contrast, with the proposed collision cost we were able to get a collision-free trajectory, as the proposed cost function pulls the trajectory by a smaller amount at each iteration, keeping the length of the trajectory smaller. Despite this, the average number of iterations needed was the same or less than with the original CHOMP.

[4] In this particular case the difference between the cylinder's diameter and the ring's one is 0.1 mm. Nevertheless, for larger differences it can be expected that the assembly process would need more steps to be accomplished, as the number of steps depends on the diameters of both the object and the cylinder.

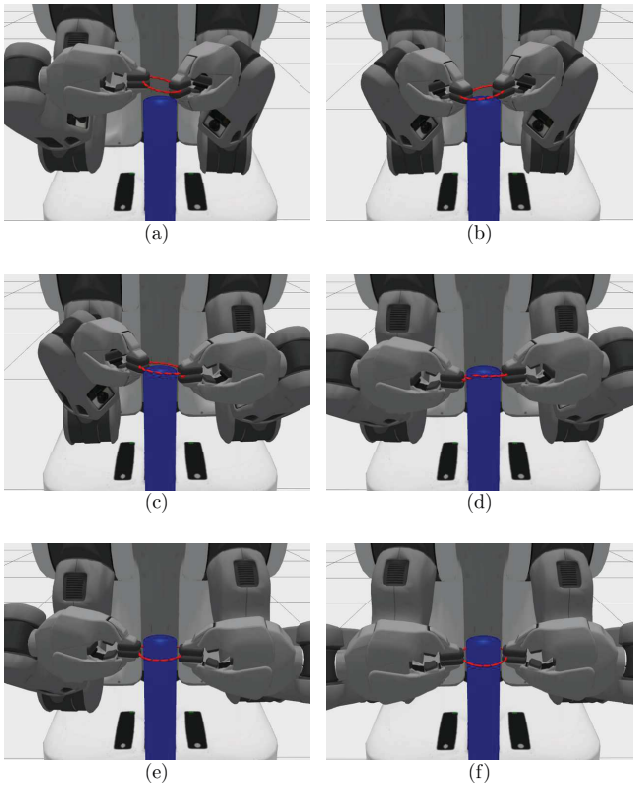

Figure 6: Assembly process in simulation at (a) end of step 1, (b) end of step 2, (c) end of step 3, (d) end of step 4, (e) end of step 5 and (f) end of step 6.

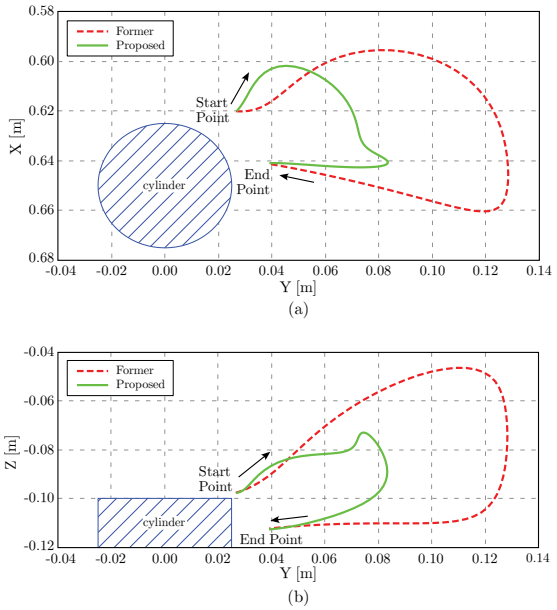

Figure 7: Robot's left gripper trajectory (at the grasping point during step 3), obtained with the original CHOMP's collision cost function given by equation (16) and the proposed collision cost given by equation (17). In (a) the X-Y plane and in (b) the Y-Z plane.

6.2 Analysis of Objective Functionals' Weights

Next, we analyzed the influence of the collision weight cost w_c in the resulting trajectory ($w_e = 0$). Fig. 8 shows the top view (X-Y plane) in (a) and the front view (Y-Z plane) in (b) of the trajectories described by the grasping position of the left gripper during step 3 of the assembly process, obtained with 4 different collision weights w_c. It can be seen that the trajectories are similar for all the values of w_c. Their collision costs, given by (15), are also similar (within 0.0001).

Fig. 9 shows the top view (X-Y plane) in (a) and the front view (Y-Z plane) in (b), of the trajectories described by the grasping position of the left gripper, obtained with the proposed collision cost function ($w_e = 0$), and obtained when adding the energy objective functional to the step planner ($w_e \neq 0$). As it can be seen, the trajectories obtained when $w_e \neq 0$ are considerably shorter and closer to the cylinder than the one with $w_e = 0$.

Similarly, Fig. 10 shows the top view (X-Y plane) in (a) and the front view (Y-Z plane) in (b), of the trajectories described by the grasping position of the right gripper during step 4 of the assembly process, obtained with the proposed collision cost function ($w_e = 0$), and obtained when adding the energy objective functional to the step planner ($w_e \neq 0$). At this assembling step, it can be seen that the trajectory obtained with $w_e = 0.0005$ describes a semicircle just as if

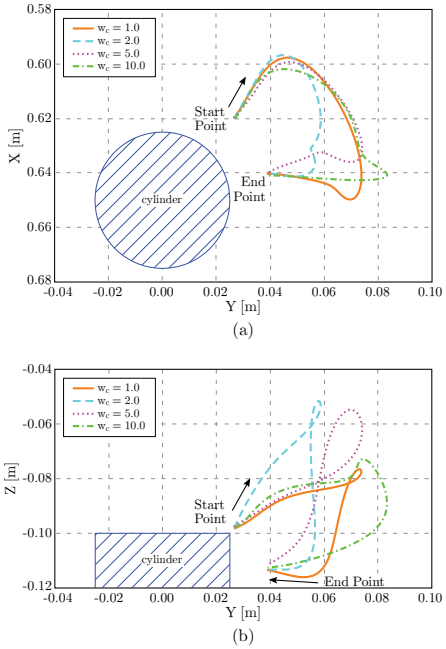

Figure 8: Robot's left gripper trajectory (at the grasping point during step 3) using the proposed collision cost function for 4 different collision weights. In (a) the X-Y plane and in (b) the Y-Z plane, for $w_e = 0$.

it was passing along the cylinder's edge. Consequently minimizing the object's deformation. In contrast, the trajectory obtained with $w_e = 0$ makes a turn around the cylinder in a similar way to the trajectory at step 3 (Fig. 9). Similar to the case shown in Fig. 9, for $w_e = 0.001$ and 0.002 the gripper moves towards the robot, avoiding the cylinder and getting closer to the opposite gripper, reducing the deformation of the elastic object.

For analyzing the influence of the objective functionals weights, several simulations were carried out. The average sum of all the collision costs (eq. 15) and all the energy costs (eq. 5) for all the steps of the assembly process (the average cost of 3 simulation runs for each combination of weights) are summarized in Table 1 for $w_e = 0.0005$, Table 2 for $w_e = 0.001$ and Table 3 for $w_e = 0.002$. The smoothness costs are not included as they are in the order of hundreds of thousands. Furthermore the largest difference among them is 0.25% of the overall average cost, which means there is no significant difference among them. It can be seen, that overall the smallest energy costs were obtained with $w_e = 0.002$, while the collision costs does not change significantly. The smallest energy cost was obtained for the combination of $w_e = 0.002$ with $w_c = 2.0$ and $w_s = 0.00001$. If we group the results by w_s instead of w_e and calculate the average energy cost, it is found that the smallest energy costs were

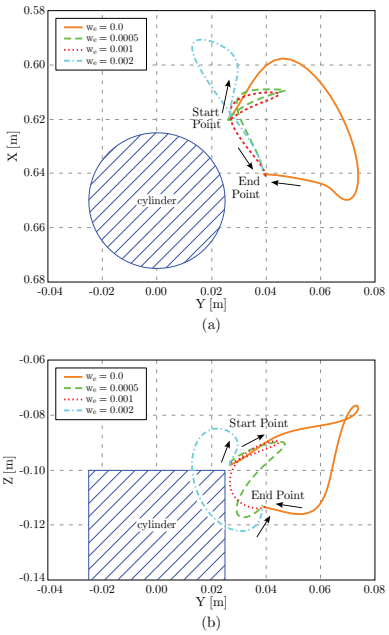

Figure 9: Robot's left gripper trajectory (at the grasping point during step 3) using the proposed step planner with and without the energy objective functional. In (a) the X-Y plane and in (b) the Y-Z plane, with $w_s = 0.00001$ and $w_c = 1.0$.

obtained with $w_s = 0.00001$. Similarly, if we group by w_c, it is found that the smallest energy costs were obtained with $w_c = 2.0$. These results coincide with the smallest energy cost obtained.

7 Experimental Results

In this section the experimental results of the proposed assembly planner using a Baxter robot are presented. For validating the proposed assembly planner we used the ring-shaped elastic objects shown in Fig. 11. The first object is a common rubber band (natural rubber), the second is an o-ring made of silicon rubber (stiffer than the rubber band), and the third is an o-ring made of nitrile rubber (also known as NBR) commonly known as a packing, which is stiffer than both the rubber band and the silicon made o-ring. Their dimensions are summarized in Table 4. The parameters given to both the sequence planner and the CHOMP algorithm are those of the nitrile-made o-ring (the stiffer of the three objects), that has a Young's modulus of ≈ 4.125 MPa (based on the o-ring's manufacturer data sheet). The parameters used in the assembly task planner are: $dz = 0.007$ and $\Delta X = 0.03$ m, and the cylinder's diameter is 5.0 cm. For comparison purposes, the joints' trajectories requested to the

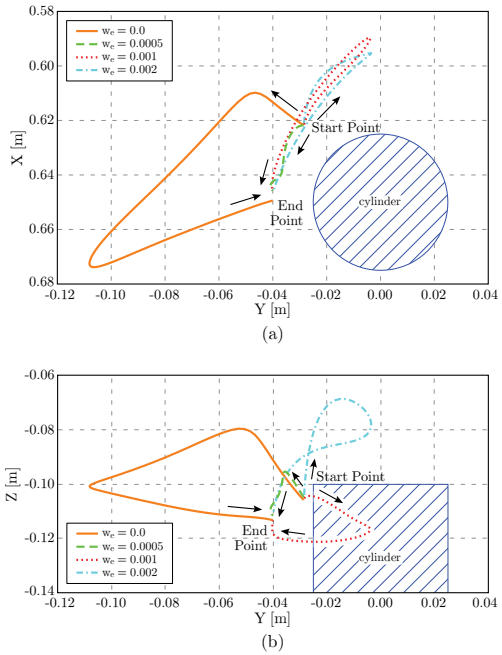

Figure 10: Robot's right gripper (at the grasping point during step 4) using the proposed step planner with and without the energy objective functional. In (a) the X-Y plane and in (b) the Y-Z plane, with $w_s = 0.00001$ and $w_c = 1.0$.

Table 1: Collision cost and energy cost for $w_e = 0.0005$.

w_s	w_c	Collision cost	Energy cost
0.000005	0.5	0.0162	17.14
	1.0	0.0133	25.92
	2.0	0.0135	22.91
0.00001	0.5	0.0165	21.40
	1.0	0.0136	20.92
	2.0	0.0140	20.04
0.00002	0.5	0.0155	18.34
	1.0	0.0141	22.51
	2.0	0.0149	25.06
Average		0.0146	21.58

robot are exactly the same for all the three objects, i.e. we only plan once (for the stiffest object, the nitrile-made o-ring) and then use the same plan for all the objects. Fig. 12 shows the snapshots of the experiments using the

Table 2: Collision cost and energy cost for $w_e = 0.001$.

w_s	w_c	Collision cost	Energy cost
0.000005	0.5	0.0153	19.42
	1.0	0.0180	15.94
	2.0	0.0142	17.90
0.00001	0.5	0.0141	20.21
	1.0	0.0153	16.20
	2.0	0.0144	15.67
0.00002	0.5	0.0150	20.99
	1.0	0.0155	19.73
	2.0	0.0136	26.60
Average		0.0150	19.18

Table 3: Collision cost and energy cost for $w_e = 0.002$.

w_s	w_c	Collision cost	Energy cost
0.000005	0.5	0.0154	18.75
	1.0	0.0142	17.74
	2.0	0.0167	15.33
0.00001	0.5	0.0155	17.83
	1.0	0.0155	17.16
	2.0	0.0170	15.22
0.00002	0.5	0.0163	16.88
	1.0	0.0161	21.25
	2.0	0.0158	16.47
Average		0.0158	17.40

rubber band. The robot accomplishes the assembly task in 24 s. (humans can do it in 5 s.), when using a discretization time of $\Delta t = 0.01$ and a trajectory length of 3 s. in the CHOMP algorithm (section 5.1), the execution time can be shorten if we use a smaller trajectory length. Also, it was verified that the robot successfully assembled all of the ring-shaped objects into the cylinder. These results suggest that by supposing that the object has a high stiffness (for the Energy cost computation purposes in the CHOMP algorithm), the obtained motion plan can work for objects with equal or less stiffness than the supposed one. Thus, we can drop out the assumption of knowing the material of the ring-shaped object and set the value of k through (8) using the Young's modulus

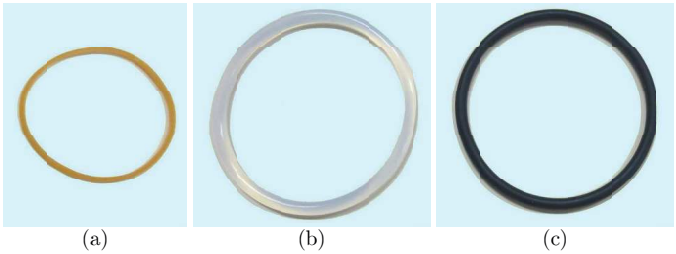

(a) (b) (c)

Figure 11: O-ring shaped objects used in experiments: a rubber band made of natural rubber (a), an o-ring made of silicon rubber (b), and an o-ring made of nitrile rubber (c).

Table 4: Dimensions of the objects shown in Fig. 11.

Object	undeformed inner diameter [mm]	thickness [mm]
rubber band	47.0	1.0
silicon o-ring	49.7	3.5
nitrile o-ring	49.4	3.0

of a known material with high stiffness. Also, it can be seen that through the entire assembly process the position of the grasping point of the object does not change significantly supporting our assumption that the robot grasps firmly the object. It should be noticed that this assumption is merely for the sake of simplicity in the computation of the object's deformation in the CHOMP algorithm. However, it does not affect the performance of the assembly planner as verified through the experiments.

Fig. 13 shows the trajectories of each of the tips of the robot's grippers in experiment (using the rubber band) and simulation compared with the desired trajectories, where the continuous, dashed and bold lines represent the experimental, simulation and desired trajectories, respectively. In this case, as it can be seen the robot's tip trajectories followed the desired ones, successfully assembling the rubber band into the cylinder. Furthermore, in this work we set the cylinder vertically, nevertheless it can also be set horizontally or in any other posture (reachable by the robot). The only modification needed would be the transformation between the coordinate system used now and the new posture, without affecting anything else.

We repeated the experiment with both the rubber band and the silicon-made o-ring 5 times in a row with each material, having succeeded in the assembly each time. In contrast with the nitrile-made o-ring we were able to do the experiment only 2 times in a row, since in the second time the designed holder

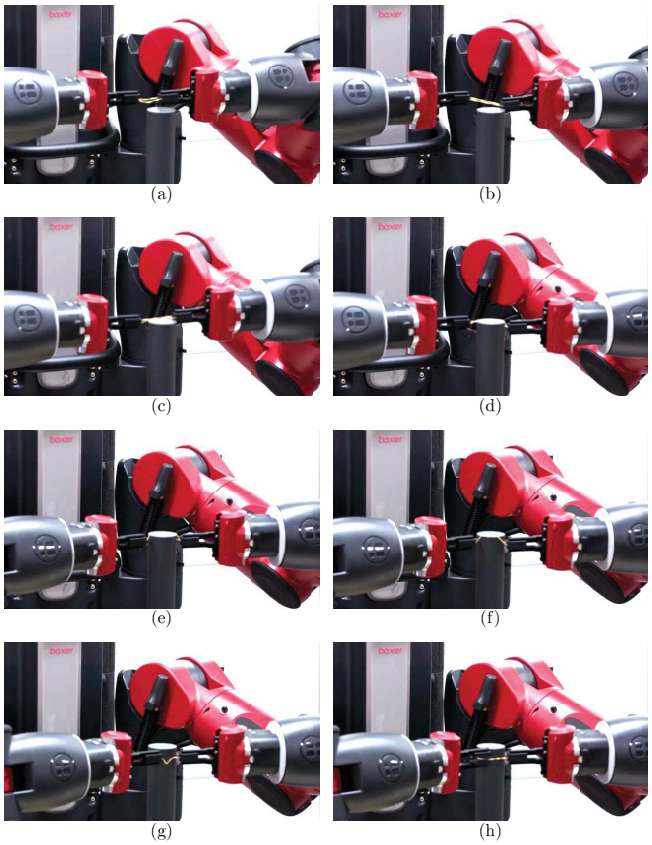

Figure 12: Snapshots of the experiment using a rubber band at (a) initial state, (b) end of step 1, (c) end of step 2, (d) end of step 3, (e) end of step 4, (f) end of step 5, (g) end of step 6 and (h) after releasing the object.

(shown in Fig. 14) for grasping the o-ring got detached from the robot's finger. This happened due to the high stiffness of the o-ring, however although the holder got detached at the last step, the o-ring was correctly inserted in the cylinder. Fig. 15 shows the average of the computed deformation of the object (using the method presented in section 5.2) in all of the experiments (5 times for the rubber band and the silicon-made o-ring and 2 times for the nitrile-made o-ring). It can be seen, that for the first steps the assembly planner is able to keep the object undeformed. Then as the object begins to be inserted (taking the shape of the cylinder), it begins to deform. At the end, it can be observed that the rubber band being the less stiffer and having the shortest perimeter, gets deformed more than the o-rings. At the last step it can be seen that the deformation of the o-rings is very similar, which means that their shape is about the same (inserted on the cylinder).

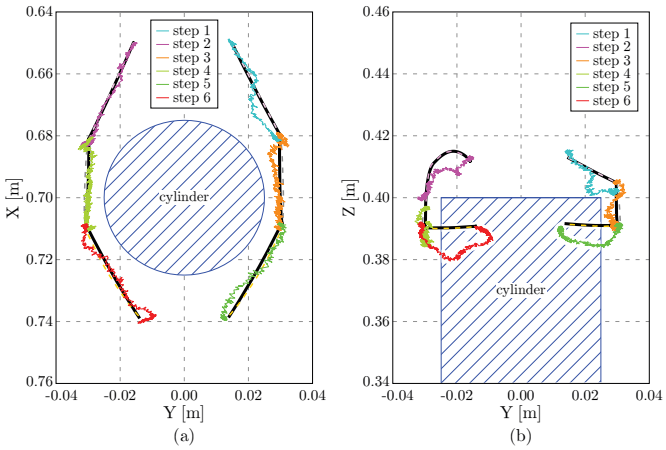

Figure 13: Tip trajectories of Baxter's grippers when the object is the rubber band. In (a) top view (X-Y plane) and in (b) front view (Y-Z plane). The continuous, dotted and dashed lines represent the experimental data, simulation data and the desired trajectories, respectively.

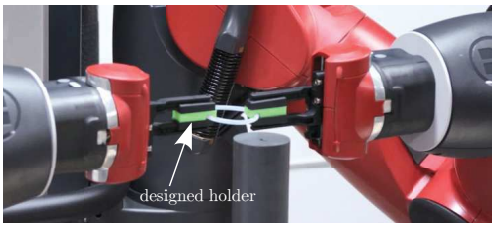

Figure 14: Robot holding the silicon-made o-ring using the designed holder

8 Conclusion

This paper discussed the assembly planning of ring-shaped elastic objects considering the object's deformation. The main results of this paper are summarized as follows:

1. We presented an assembly task planner for a dual-arm robot that computes key poses of the robot to successfully accomplish the assembly task of a ring-shaped object into a cylinder.
2. We introduced an energy objective functional that minimized the deformation of the elastic object when manipulated by a dual-arm robot.
3. We introduced a less strict collision cost function that allows the robot to be near to its environment without colliding. This function proved that it can yield collision-free trajectories.
4. We showed that the addition of the energy-based objective functional to the original CHOMP method is effective for minimizing the elastic energy of the object through several simulations.

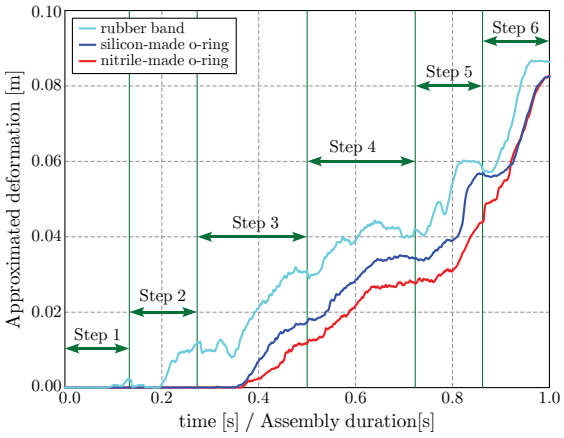

Figure 15: Average of the computed deformation of each of the objects in experiments.

5. We examined the influence of the objective functionals weights, and found that for the smoothness and collision costs there are no significant differences. In contrast, for the energy cost, a combination of weights yielding the smallest energy cost was found.
6. We confirmed the validity of the proposed assembly planner through experiments using three different elastic ring-shaped objects.

This work is considered to be the basis for accomplishing other types of assembly tasks involving deformable objects. In the future we would like to discuss assembly tasks that required the ring-shaped object to be placed in an specific part of the cylinder and/or on another object and how to pick/grasp the ring-shaped objects autonomously. Also, we would like to discuss other methods to achieve the assembly task of elastic objects that have different shapes.

References

Atkinson, J. (2012), 'Engineer who opposed challenger launch offers personal look at tragedy', The Researcher News, National Aeronautics and Space Administration (NASA).
`https://www.nasa.gov/centers/langley/news/researchernews/rn_Colloquium1012.html`.

Bretl, T. & McCarthy, Z. (2014), 'Quasi-static manipulation of a Kirchhoff elastic rod based on a geometric analysis of equilibrium configurations', *International Journal of Robotics Research (IJRR)* **33**(1), 48–68.

Friedrich, W., Lim, P. & Nicholls, H. (1996), Sensory gripping system for variable products, *in* 'IEEE International Conference on Robotics and Automation (ICRA)', Vol. 4, Minneapolis, MN, pp. 3324–3329.

Kalakrishnan, M., Chitta, S., Theodorou, E., Pastor, P. & Schaal, S. (2011), STOMP: Stochastic Trajectory Optimization for Motion Planning, *in* 'IEEE International Conference on Robotics and Automation (ICRA)', Shanghai, China, pp. 4569–4574.

Karaman, S. & Frazzoli, E. (2010), 'Incremental sampling-based algorithms for optimal motion planning', *Robotics Science and Systems VI* **104**.

Karaman, S. & Frazzoli, E. (2011), 'Sampling-based algorithms for optimal motion planning', *International Journal of Robotics Research (IJRR)* **30**(7), 846–894.

Kavraki, L. E., ˇ Svestka, P., Latombe, J.-C. & Overmars, M. H. (1996), 'Probabilistic roadmaps for path planning in high-dimensional configuration spaces', *IEEE Trans. on Robotics and Automation* **12**(4), 566–580.

Lamiraux, F. & Kavraki, L. E. (2001), 'Planning paths for elastic objects under manipulation constraints', *International Journal of Robotics Research (IJRR)* **20**(3), 188–208.

LaValle, S. M. & Kuffner Jr, J. J. (2001), 'Randomized kinodynamic planning', *The international journal of robotics research* **20**(5), 378–400.

Masehian, E. & Sedighizadeh, D. (2007), 'Classic and heuristic approaches in robot motion planning-a chronological review', *World Academy of Science, Engineering and Technology* **23**, 101–106.

Miura, J. & Ikeuchi, K. (1995), Assembly of flexible objects without analytical models, *in* 'IEEE/RSJ International Conference on Intelligent Robots and Systems (IROS)', Vol. 2, Pittsburgh, PA, pp. 77–83.

Miura, J. & Ikeuchi, K. (1998), 'Task planning of assembly of flexible objects and vision-based verification', *Robotica* **16**(3), 297–307.

Moll, M. & Kavraki, L. E. (2006), 'Path planning for deformable linear objects', *IEEE Trans. on Robotics* **22**(4), 625–636.

Nakagaki, H., Kitagaki, K., Ogasawara, T. & Tsukune, H. (1997), Study of deformation and insertion tasks of a flexible wire, *in* 'IEEE International Conference on Robotics and Automation (ICRA)', Albuquerque, NM, pp. 2397–2402.

Quinlan, S. (1994), Real-time modification of collision-free paths, PhD thesis, Stanford University.

Rambow, M., Schauß, T., Buss, M. & Hirche, S. (2012), Autonomous manipulation of deformable objects based on teleoperated demonstrations, *in* 'IEEE/RSJ International Conference on Intelligent Robots and Systems (IROS)', Vilamoura, Portugal, pp. 2809–2814.

Ramirez-Alpizar, I. G., Harada, K. & Yoshida, E. (2014), Motion planning for dual-arm assembly of ring-shaped elastic objects, *in* 'IEEE/RAS International Conference on Humanoid Robotics (Humanoids)', Madrid, Spain, pp. 594–600.

Saha, M. & Isto, P. (2007), 'Manipulation planning for deformable linear objects', *IEEE Trans. on Robotics* **23**(6), 1141–1150.

Sakamoto, N., Higashimori, M., Tsuji, T. & Kaneko, M. (2007), An optimum design of robotic hand for handling a visco-elastic object based on Maxwell model, *in* 'IEEE International Conference on Robotics and Automation (ICRA)', Rome, Italy, pp. 1219–1225.

Shoushtari, A. L., Leylavi Shoushtari, A., Mazzoleni, S., Mazzoleni, S., Dario, P. & Dario, P. (2016), 'Bio-inspired kinematical control of redundant robotic manipulators', *Assembly Automation* **36**(2), 200–215.

Villareal, A. & Asada, H. (1991), A geometric representation of distributed compliance for the assembly of flexible parts, *in* 'IEEE International Conference on Robotics and Automation (ICRA)', Vol. 3, Sacramento, CA, pp. 2708–2715.

Vinh, T. V., Tomizawa, T., Kudoh, S. & Suehiro, T. (2012), A new strategy for making a knot with a general-purpose arm, *in* 'IEEE International Conference on Robotics and Automation (ICRA)', Saint Paul, MN, pp. 2217–2222.

Wakamatsu, H., Hirai, S., & Iwata, K. (2004), Static analysis of deformable object grasping based on bounded force closure, *in* 'IEEE/RSJ International Conference on Intelligent Robots and Systems (IROS)', Vol. 2, New Orleans, LA, pp. 1719–1725.

Wakamatsu, H., Tsumaya, A., Arai, E., & Hirai, S. (2006), Manipulation planning for unraveling linear objects, *in* 'IEEE International Conference on Robotics and Automation (ICRA)', Orlando, Florida, pp. 2485–2490.

Wakamatsu, H., Tsumaya, A., Arai, E. & Hirai, S. (2004), Planning of one-handed knotting/raveling manipulation of linear objects, *in* 'IEEE International Conference on Robotics and Automation (ICRA)', Vol. 2, New Orleans, LA, pp. 1719–1725.

Wang, W., Bell, M. P. & Balkcom, D. (2015), 'Towards arranging and tightening knots and unknots with fixtures', *IEEE Trans. on Automation Science and Engineering* **12**(4), 1318–1331.

Wolter, J. & Kroll, E. (1996), Toward assembly sequence planning with flexible parts, *in* 'IEEE International Conference on Robotics and Automation (ICRA)', Minneapolis, MN, pp. 1517–1524.

Yamakawa, Y., Namiki, A. & Ishikawa, M. (2010), Motion planning for dynamic knotting of a flexible rope with a high-speed robot arm, *in* 'IEEE/RSJ International Conference on Intelligent Robots and Systems (IROS)', Taipei, Taiwan, pp. 49–54.

Yamakawa, Y., Namiki, A. & Ishikawa, M. (2012), Simple model and deformation control of a flexible rope using constant, high-speed motion of a robot arm, *in* 'IEEE International Conference on Robotics and Automation (ICRA)', Saint Paul, MN, pp. 2249–2254.

Yoshida, E., Ayusawa, K., Ramirez-Alpizar, I. G., Harada, K., Duriez, C. & Kheddar, A. (2015), Simulation-based optimal motion planning for deformable object, *in* 'IEEE International Workshop on Advanced Robotics and its Social Impacts (ARSO)'.

Yue, S. & Henrich, D. (2002), Manipulating deformable linear objects: sensor-based fast manipulation during vibration, *in* 'IEEE International Conference on Robotics and Automation (ICRA)', Washington, DC, pp. 2467–2472.

Zheng, Y. F., Pei, R. & Chen, C. (1991), Strategies for automatic assembly of deformable objects, *in* 'IEEE International Conference on Robotics and Automation (ICRA)', Vol. 3, Sacramento, CA, pp. 2598–2603.

Zucker, M., Ratliff, N., Dragan, A. D., Pivtoraiko, M., Klingensmith, M., Dellin, C. M., Bagnell, J. A. & Srinivasa, S. (2013), 'CHOMP: Covariant hamiltonian optimization for motion planning', *International Journal of Robotics Research (IJRR)* **32**(9-10), 1164–1193.